INSTITUT DE FRANCE
Académie des sciences

Comptes Rendus

Physique

Clément Dutreix, Hector González-Herrero, Ivan Brihuega, Mikhail I. Katsnelson, Claude Chapelier and Vincent T. Renard

Measuring graphene's Berry phase at $B = 0$ T

Volume 22, Special Issue S4 (2021), p. 133-143

Published online: 8 September 2021
Issue date: 8 March 2022

https://doi.org/10.5802/crphys.79

Part of Special Issue: Recent advances in 2D material physics
Guest editors: Xavier Marie (INSA Toulouse, Université Toulouse III Paul Sabatier, CNRS, France) and Johann Coraux (Institut Néel, Université Grenoble Alpes, CNRS, France)

Les Comptes Rendus. Physique *sont membres du Centre Mersenne pour l'édition scientifique ouverte*
www.centre-mersenne.org
e-ISSN : 1878-1535

Comptes Rendus
Physique
2021, 22, nº S4, p. 133-143
https://doi.org/10.5802/crphys.79

Recent advances in 2D material physics / *Physique des matériaux bidimensionnels*

Measuring graphene's Berry phase at $B = 0$ T

Mesurer la phase de Berry du graphène en l'absence de champ magnétique

Clément Dutreix [a], **Hector González-Herrero** [b, c], **Ivan Brihuega** [b, c, d], **Mikhail I. Katsnelson** [*, e], **Claude Chapelier** [f] **and Vincent T. Renard** [*, f]

[a] Université de Bordeaux, France and CNRS, LOMA, UMR 5798, Talence, F-33400, France

[b] Departamento de Física de la Materia Condensada, Universidad Autónoma de Madrid, E-28049 Madrid, Spain

[c] Condensed Matter Physics Center (IFIMAC), Universidad Autónoma de Madrid, E-28049 Madrid, Spain

[d] Instituto Nicolás Cabrera, Universidad Autónoma de Madrid, E-28049 Madrid, Spain

[e] Radboud University, Institute for Molecules and Materials, Nijmegen, The Netherlands

[f] Univ. Grenoble Alpes, CEA, Grenoble INP, IRIG, PHELIQS, F-38000 Grenoble, France

E-mails: clement.dutreix@u-bordeaux.fr (C. Dutreix), hector.gonzalezherrero@aalto.fi (H. González-Herrero), ivan.brihuega@uam.es (I. Brihuega), M.Katsnelson@science.ru.nl (M. I. Katsnelson), claude.chapelier@cea.fr (C. Chapelier), vincent.renard@cea.fr (V. T. Renard)

Abstract. The Berry phase of wave functions is a key quantity to understand various low-energy properties of matter, among which electric polarisation, orbital magnetism, as well as topological and ultra-relativistic phenomena. Standard approaches to probe the Berry phase in solids rely on the electron dynamics in response to electromagnetic forces. In graphene, probing the Berry phase π of the massless relativistic electrons requires an external magnetic field. Here, we show that the Berry phase also affects the static response of the electrons to a single atomic scatterer, through wavefront dislocations in the surrounding standing-wave interference. This provides a new experimental method to measure the graphene Berry phase in the absence of any magnetic field and demonstrates that local disorder can be exploited as probe of topological quantum matter in scanning tunnelling microscopy experiments.

Résumé. Les interférences de quasiparticules observées par microscopie à effet tunnel sont particulièrement utiles pour étudier les propriétés électroniques de matériaux en surfaces. Ces interférences possèdent des informations sur la surface de Fermi du système et leur résolution en énergie permet, dans certains cas, de reconstruire la relation dispersion. Nous montrons ici que les images d'interférences de quasiparticules peuvent aussi contenir une information sur la phase de Berry qui caractérise la structure de bande du

* Corresponding authors.

matériau. La phase de Berry est une phase géométrique que les fonctions d'onde electroniques acquièrent lors d'une évolution cyclique dans un espace de paramètres. Elle est quantifiée lorsque la trajectoire de l'évolution ensèrre une singularité des fonctions d'onde. Il s'agit alors d'une propriété topologique de la structure de bande. La phase de Berry dans les solides est traditionnellement mesurée en appliquant des champs électromagnétiques pour forcer les particules à former de trajectoires fermées. L'utilisation de la figure d'interférence de quasiparticules permet de s'extraire de ce paradigme car la phase de Berry peut affecter la réponse statique des électrons au désordre en l'absence de champ électromagnétique.

Keywords. Berry phase, Graphene, STM, Wavefront dislocations, Topology, Atomic defect.

Mots-clés. Phase de Berry, Graphène, Microscope à effet tunnel, Topologie, Interférence de quasi-particules, Défaut atomique.

Available online 8th September 2021

1. Introduction

In quantum mechanics, the phase of the wave function is (locally) arbitrary. This U(1) gauge invariance nonetheless allows observable manifestations of the wave-function phase through cyclic evolutions. A spectacular example is the demonstration of the physical relevance of the magnetic vector potential in quantum mechanics, when a charged particle orbits around a thread of magnetic flux. In this experiment, the Aharonov–Bohm phase evidences the existence of the magnetic flux without the particle ever passing through it [1]. Another fundamental illustration concerns the adiabatic journey of a wave function in some parameter space. If the wave function comes back to the initial state, it may have accumulated a phase shift that is reminiscent of the geometry of its trip in Hilbert space. This geometrical quantity is known as Berry phase [2]. Similarly to the Aharonov–Bohm phase, it is gauge invariant and leads to observable effects. On his way to the discovery of this geometrical phase, Berry was concerned with spectral degeneracies in two dimensions [3]: "*[…] These degeneracies require two parameters—one is in general not sufficient to produce a degeneracy—and in terms of these parameters the energy levels are sheets in the form of a double cone. The double cone is also called a diabolo (after a spinning toy of the same shape), so I called the intersections "diabolical points". But how can we know that the two sheets really touch, rather than avoiding each other as energy levels typically do when just one parameter is varied? In 1978 I found the criterion: while encircling a diabolical point in the space of parameters, each of the two wave functions, when smoothly continued round its sheet, must change sign*". In other words, the wave functions accumulate a π quantized phase shift along its journey provided it encloses a diabolic degeneracy point. The Berry phase is then topological in this case.

The spectral degeneracies described by Berry exist in the band structure of graphene, in which the Dirac cones are the diabolo and the Dirac points the diabolical points. As a consequence the waves functions also pick a π Berry phase when travelling around a Dirac point. This topological feature of graphene's band structure has been demonstrated beautifully for electrons confined in whispering gallery modes in this material [4]. In a semi-classical picture, the confined electrons can be viewed as bouncing from circular p–n junctions created by the electrostatic potential of a Scanning Tunnelling Microscope (STM) tip or a charge embedded in the substrate. They perform loops that do not enclose the Dirac points in momentum space. These trajectories can be engineered to enclose a Dirac point with a small perpendicular magnetic field. The inclusion provokes abrupt changes in the energy spectrum of the resonator. Such spectral features result from the π-quantised Berry phase picked up by the wave functions orbiting around a Dirac point. More generally, the Berry phase associated with magnetic cyclotron orbits around a Dirac point shifts the energy of the Landau levels, the magneto-oscillations, and the Hall conductivity that becomes anomalously quantised on half-integer values of the conductance quantum [5,6].

The present article presents an alternative approach to access the Berry phase of graphene in the absence of magnetic field. It relies on disorder-induced standing-wave interference resolved in scanning tunnelling microscopy (STM).

2. Quasiparticle interference: measurements of energy bands with a STM

The determination of energy bands with an STM has history which starts in the early days of this technique [7–10]. In a STM experiment, the tunneling current between the STM tip and the conducting surface of a material provides access to the local density of states of the surface (LDOS). The later can fluctuate near defects to form a standing wave usually called a Quasi-Particle Interference (QPI). The LDOS fluctuations around a single impurity have characteristic features informative of the host material. They exhibit long-range oscillations that decay algebraically with the distance r to the impurity. The characteristic wavelength of the oscillations is $1/q_{\mathrm{F}}$, where q_{F} is the Fermi wavevector. For the two-dimensional electron gases realized on some surfaces of noble metals, the LDOS fluctuations asymptotically behave as

$$\delta\rho(\mathbf{r},E) \propto \frac{1}{q_{\mathrm{F}} r}\cos(2q_{\mathrm{F}} r), \tag{1}$$

where we omit any phase shift for simplicity. They are often referred to as (energy-resolved) Friedel oscillations in hommage to French physicist Jacques Friedel who predicted the long-range oscillations of the electron density screening charged impurities in metals [11]. The Fourier-transformed local density of states (FT-LDOS) offers a clear connection to the iso-energy contours of the band structure in momentum space. Indeed, the Fourier transform of (1) outlines a $2q_{\mathrm{F}}$-radius ring in Fourier space mapping the circular Fermi surface of radius q_{F} [9]. This mapping shows that elastic backscattering is the most efficient scattering process. Since the STM can also measure the standing wave at any energy $E_{\mathrm{F}} - eV_b$ (V_b is the tip-surface bias), it also enables the resolution of the parabolic dispersion relation of the electron gas at low energy. Thus, the LDOS fluctuations are informative about the energy bands of materials. As such QPI have been widely used to study the band structure of novel materials [12].

3. Graphene's pseudospin evidenced in QPI

After the discovery of graphene, researchers realized that QPI could also be informative on the pseudospin of the wave functions. The low-energy properties of the massless relativistic electrons in graphene are well described by the following Hamiltonian matrix

$$H(\mathbf{K}+\mathbf{q}) \simeq \begin{pmatrix} 0 & v_{\mathrm{F}}\xi\, q\mathrm{e}^{\mathrm{i}\xi\theta_{\mathbf{q}}} \\ v_{\mathrm{F}}\xi\, q\mathrm{e}^{-\mathrm{i}\xi\theta_{\mathbf{q}}} & 0 \end{pmatrix}, \tag{2}$$

written in the sublattice basis (A,B). The Fermi velocity is $v_{\mathrm{F}} \simeq 10^6$ m·s^{-1}. The index $\xi = \pm 1$ labels the two nonequivalent valleys at $\pm\mathbf{K}$ in the Brillouin zone, while q and $\theta_{\mathbf{q}}$ denote the norm and polar angle of wave vector $\mathbf{q}$ with respect to direction x (cf. Figure 1). The dispersion relation is conical $E_{\pm}(\mathbf{K}+\mathbf{q}) \simeq \pm v_{\mathrm{F}} q$ and the eigenstates satisfy $\sqrt{2}\,|u_{\pm}(\mathbf{K}+\mathbf{q})\rangle = |A\rangle \mp \xi\,\mathrm{e}^{-\mathrm{i}\xi\theta_{\mathbf{q}}}|B\rangle$. The spinor structure results from the two sublattices and refers to the pseudospin $\sigma = (\xi\cos(\theta_{\mathbf{q}}), \sin(\theta_{\mathbf{q}}), 0)$ represented in Figure 1c. A remarkable property of the electron wave-functions in graphene is the lock-in relation between the sublattice pseudospin and the wave vector.

Figure 2 illustrates how QPI measurements in STM have proven the existence of the wave-function pseudospin [13–15]. Figure 2a shows a large STM image recorded on a single layer of graphene, grown on the silicon face of SiC [15]. A single atomic impurity induces both intravalley and intervalley elastic scattering. Similarly to the noble metals, the iso-energy contour of each valley has a circular geometry at low energy. A naive expectation is that intravalley scattering and

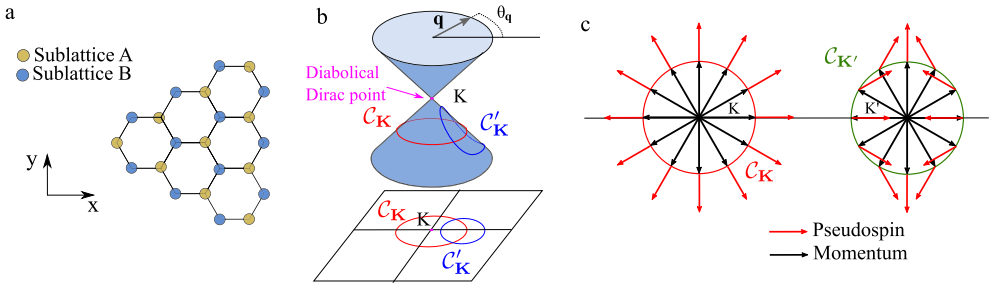

Figure 1. (a) The bipartite hexagonal lattice of graphene. (b) Dirac cone at the K point. $\mathscr{C}_K$ and $\mathscr{C}'_K$ re present two types of closed trajectories in reciprocal space enclosing (resp. not enclosing) the Dirac point (Adapted from Ref. [4]). (c) Graphene's pseudospin is locked on momentum but does not have the same texture in the two valleys.

intervalley scattering should both yield a $2q_{\mathrm{F}}$-radius ring in Fourier space. Nevertheless, such a ring is absent for intravalley scattering (Figure 2d), while for intervalley scattering, the ring is present but shows pronounced extinctions in the directions perpendicular to Γ**K** (Figure 2e–g). It turns out that the pseudospin texture in each valley allows a geometrical explanation of these two observations.

The pseudospin texture shown in Figure 1c imposes that the pseudo spin has to flip in intravalley backscattering. Figure 2j illustrates this for a particular direction. This π rotation of the pseudospin induces a $\pi/2$ rotation of the wave-function spinor in Hilbert space, and so the term $\langle u_{\pm}(K-q)|u_{\pm}(K+q)\rangle = 0$ yields destructive interference [16]. The absence of intravalley backscattering in graphene has profound consequences as it is responsible for Klein tunneling through smooth potential barriers [17]. In the case of a sharp atomic potential barrier, the absence of backscattering removes the $2k_{\mathrm{F}}$-radius ring in the Fourier transform of the QPI. In real space, this corresponds equivalently to the absence of the leading $1/r$-decaying Friedel oscillations, leaving an unconventional decay of $1/r^2$ in the intravalley scattering QPI [14, 18, 19]. This strong suppression of the intravalley signal makes it hardly observable in practice.

The situation is different for intervalley scattering. The two valleys have different pseudospin textures (Figure 1c). In general, intervalley backscattering between states of wave vectors parallel to **KK**′ does not require the pseudospin to flip and is therefore allowed (Figure 2j). Nevertheless, backscattering is forbidden in a specific direction, where the scattering wave vectors are perpendicular to **KK**′ (Figure 2j). This explains the extinctions observed in intervalley backscattering (Figure 2e–g) and shows that they too are manifestations of the wave-function pseudospin. Similarly to noble metals, the $2k_{\mathrm{F}}$-radius ring due to intervalley backscattering also allows the resolution of the dispersion relation at low energy [13, 15]. This is shown in Figure 2h, i and clearly highlights the linear dispersion relation with expected Fermi velocity $v_{\mathrm{F}} \simeq 10^6$ m·s.

Therefore, the absence of intravalley back scattering signal and the peculiar intervalley backscattering signal observed in the QPI in graphene are evidences of the wave-function pseudospin. The importance of such observations is at least twofold. First, they confirm that the sublattice atomic structure (distances of a few angstroms) is responsible for the pseudospin physics of the electron wave-function at low energy (wavelengths of a few tens of nanometers). Second, they also demonstrate the ability of the STM technics to probe wave-function properties, in addition to the spectral ones. Now we show that the QPI can also reveal the topological Berry phase of the electron wave-functions associated with the diabolical Dirac points in the band structure.

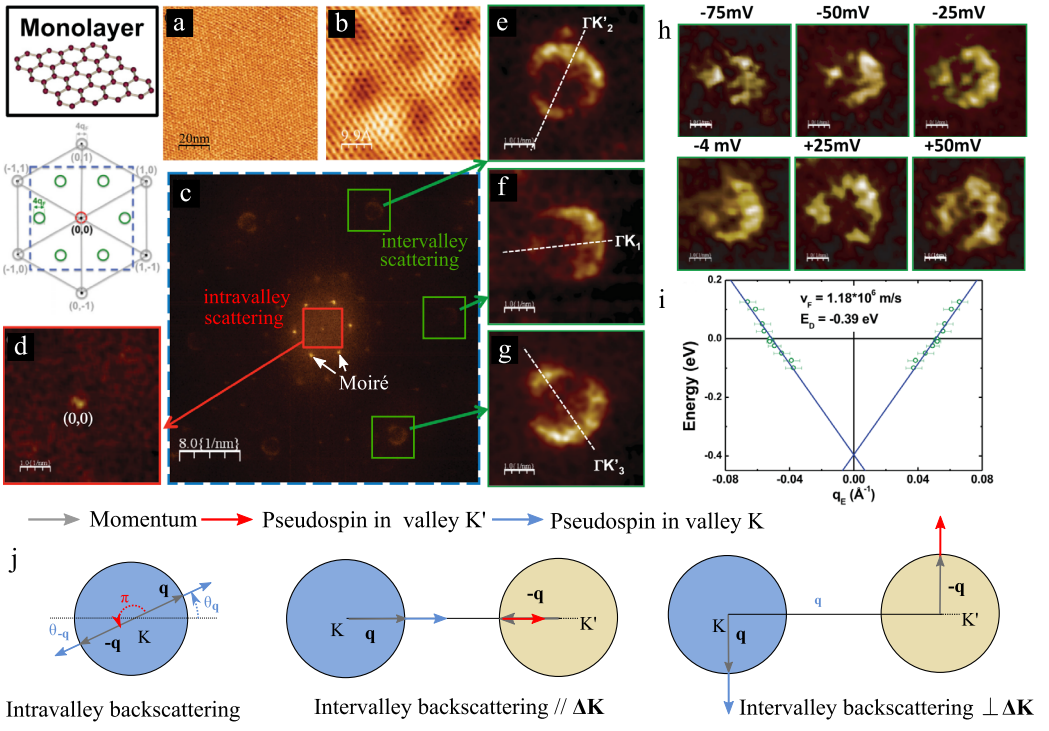

Figure 2. (a) STM image of a graphene layer grown on the silicon face of SiC. The observed periodicity is related to a moiré caused by the substrate and not relevant here. (b) Numerical zoom in the image showing atomig resolution. (c) Fast Fourrier transform of the image presented in panel (a). (d) Zoom in the center of the FFT showing no signal related to intravalley scattering. (e–g) Zoom in the FFT at position of intervalley scattering signal. Clear extinctions are observed perpendicular to the Γ**K** direction. (h) Intervalley scattering signal measured for different energies. (i) The dispersion of graphene reconstructed from the measurement of the ring diameter in panel (h). (j) Intra- and intervalley back scattering explaining the observations above. The figure is adapted from Ref. [15].

4. Wave-function Berry phase in graphene QPI

4.1. *Berry phase in graphene*

The π-quantised Berry phase γ gained by the wave functions along an orbit $\mathscr{C}_{\mathbf{K}}$ that encloses a "diabolical" Dirac point (see Figure 1b) can be calculated from Berry's definition:

$$\gamma = \mathrm{i}\oint_{\mathscr{C}_{\mathbf{K}}} \langle u_{\pm}(\mathbf{K}+\mathbf{q})|\nabla_{\mathbf{q}} u_{\pm}(\mathbf{K}+\mathbf{q})\rangle \cdot \mathrm{d}\mathbf{q} = \frac{1}{2}\oint_{\mathscr{C}_{\mathbf{K}}} \mathrm{d}(\xi\theta_{\mathbf{q}}) = \xi\pi. \tag{3}$$

For a given valley ξ, the Berry phase does not depend on details of the orbit $\mathscr{C}_{\mathbf{K}}$. It only depends on whether the orbit encloses the Dirac point or not, which makes the Berry phase not only geometrical but also topological. Importantly, the Berry phase relates directly to the pseudospin winding, as expressed by the second equality in (3). Measuring the pseudospin winding is therefore equivalent to measuring the Berry phase. This is precisely what is done in magneto-transport experiments where the pseudospin winding along cyclotron orbits around a Dirac point lead to the anomalous Quantum Hall Effect [20].

While the absence of backscattering observed in the STM experiments proves the pseudospin of wave-function exist, there remains to determine if the wave-function Berry phase can also be extracted from QPIs. Since the Berry phase is a manifestation of the wave-function phase allowed by the U(1) gauge, phase coherence is crucial in the experiment. The STM images shown in Figure 2 have a large area (100×100 nm^2). If this improves the signal-to-noise ratio and long wave-length measurements, the phase coherence is blurred by more atomic scatterers. Instead, we can exploit the local nature of the LDOS observable and resolve the QPI around a single atomic scatterer.

4.2. *Wavefront dislocations in STM images*

There are several ways to create atomic scatterers in graphene. Electron and ion bombardments can induce structural defects such as vacancies [21–23]. One can also use another approach consisting in absorbing atoms and molecules at the surface of graphene [24–27]. Here, we focus on hydrogen adatoms chemisorbed on graphene. They form covalent bonds with the p_z orbitals of the carbon atoms. The hydrogenated carbon atoms then become mainly unavailable for the conduction electrons [28, 29] making it similar to a vacancy. Contrary to vacancies that imply structural reorganisations of the neighbouring atoms in pentagones, the H adatom locally preserves the honeycomb structure. This allows the control of their positions on the graphene surface with a STM tip [30].

Figure 3a presents a STM topography image of a single H adatom on graphene. Far from the bright protrusion, the effect of the H adatom vanishes, which highlights the pristine hexagonal lattice. Closer to the adatom, an other periodic signal develops associated with a wavelength of 3.7 Å. This wavelength is characteristic of intervalley scattering, as confirmed by spectroscopic measurements. The energy-resolved image of the LDOS in Figure 3b also captures the 3.7 Å-wavelength modulations of the topographic signal. To visualise the LDOS fluctuations of wavelength 3.7 Å more clearly, one can filter the intervalley signal out from other scattering wavevectors in Fourier space. For a specific direction of intervalley scattering, this results in the LDOS fluctuations shown in Figure 3d. Now the interference fringes of wavelength 3.7 Å are clearly visible in real space. They also reveal a very striking pattern around the H adatom with the presence of two wavefront dislocations.

The dislocations in the wavefronts of the LDOS fluctuations are already visible in the raw STM images, so they are not artefacts of the filter we use in Fourier space. Figure 3d, for instance, shows that the wavefronts are identical before and after the filtering procedure for a given direction of intervalley scattering. Figures 3e, f also show that the interference fringes do not disperse with the energy and that the dislocations are a stable feature of the electronic structure at low energy.

4.3. *The dislocation strength is a measure of the Berry phase*

From the STM evidence of the absence of backscattering in graphene, we know that the rotation of the pseudospin has observable effects in the QPI. Then, let us see how the pseudospin rotates in intervalley backscattering and could affect the QPI. The orientation of the STM tip at point M supports the cylindrical representation $(r, \theta_{\mathbf{r}})$, where r is the distance to the H adatom and $\theta_{\mathbf{r}}$ is the polar angle with respect to the (O, x) axis aligned to the $\Delta\mathbf{K}$ direction (Figure 4a, b). The backscattering signal at point M results from the interference between an incoming wave of wave-vector orientation $\theta_{\mathbf{q}} = \theta_{\mathbf{r}} - \pi$ and a reflected wave of wave-vector orientation $\theta_{-\mathbf{q}} = \theta_{\mathbf{q}} + \pi = \theta_{\mathbf{r}}$. Due to the lock-in relation between the wave-vector and pseudospin orientations, we find that the pseudospin rotation is $-2\theta_{\mathbf{q}} = -2\theta_{\mathbf{r}}$ for intervalley backscattering (Figure 4a).

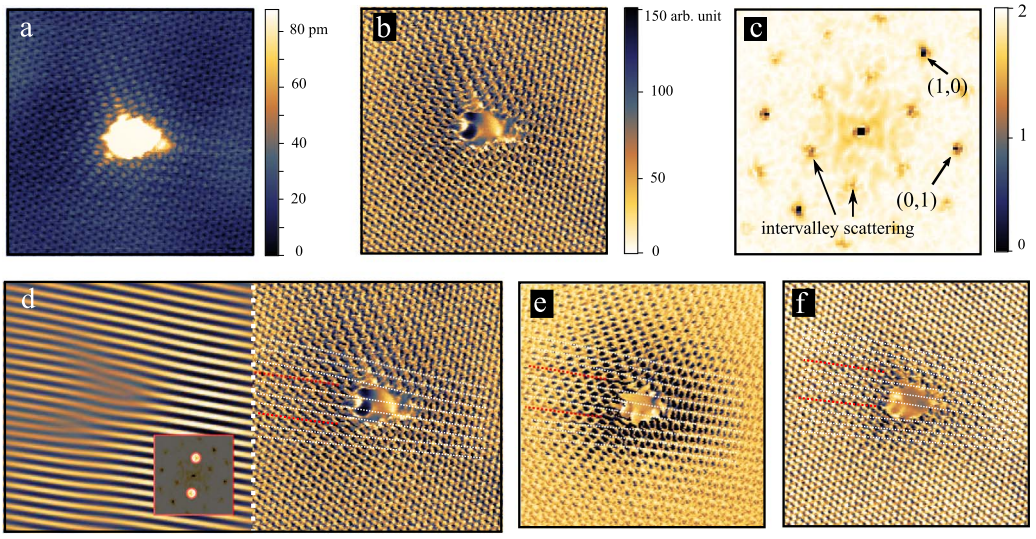

Figure 3. (a) STM topography image of an hydrogen adatom at the surface of graphene. The image is 8×8 nm^2. The bias is $V_b = 200$ mV and the tunnel current is $i_t = 5$ pA. (b) Local density of states image of the same atom at the same energy. (c) Modulus of the Fourier transform of the STM image presented in (b). The image is 78.5 nm^{-1} $\times$ 78.5 nm^{-1}. (d) The local density of states image of panel (b) is fourier filtered to reveal the intervalley backscattering interference. The inset shows the filter used. The right part shows the raw image in which dotted lines highlight the wave fronts. Equivalent result are obtained by filtering along the other directions of intervalley backscattering. (e, f) Energy resolved images measured at $V_b = 50$ mV and $V_b = -300$ mV respectively the wavefront for one direction of inter-valley scattering. The red dotted lines correspond to the additional wavefronts. Similar results are obtained in the other directions.

The wave-vector rotation between the incident and reflected waves is also locked on the tip orientation around the adatom. By moving the STM tip around the H adatom, we then probe (twice) the pseudospin winding of the incident electron along an orbit that encloses a Dirac point in reciprocal space. This is analogous to the magnetic cyclotron orbits induced by a perpendicular magnetic field. Since $\theta_{\mathbf{r}}$ winds by 2π when the tip circulates around the H atom it follows that the pseudospin rotation is 4π. This is in agreement with the two additional wave fronts inserted in the standing wave to accommodate for this phase picked up in the intervalley scattering process when circulating around the adatom. This measure of the pseudospin winding around a Dirac cone equivalently constitutes a direct measurement of the Berry phase in real space.

To support this explanation, we further describe the impurity scattering of the massless relativistic electrons within a T-matrix approach based on Green functions [31]. This diagrammatic perturbation approach leads to an analytical solution for on-site potentials, regardless of the potential strength. Thus, it enables the description of realistic point scatterers in graphene. For a H adatom on sublattice A, the surrounding electronic density reads:

$$\delta\rho(\Delta\mathbf{K},\mathbf{r},V_b) = \delta\rho_A(r,V_b)\cos(\Delta\mathbf{K}\cdot\mathbf{r}) + \xi\xi'\delta\rho_B(r,V_b)\cos(\Delta\mathbf{K}\cdot\mathbf{r} - (\xi-\xi')\theta_{\mathbf{r}}), \tag{4}$$

where V_b is the local bias applied between the STM and the graphene sheet. The two terms on the right-hand side describe the electron density on sublattices A and B, respectively. The asymptotic behaviours of $\delta\rho_A$ and $\delta\rho_B$ characterise isotropic Friedel oscillations. One recovers

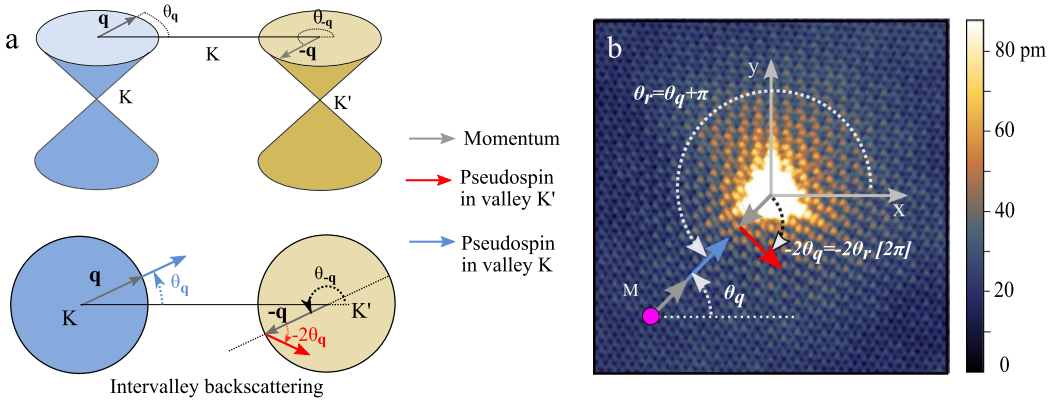

Figure 4. (a) Backscattering process in graphene. Intervalley backscattering between wavevector states $\mathbf{q}$ and $-\mathbf{q}$ belonging to nearest-neighbour valleys $\mathbf{K}$ and $\mathbf{K}'$ leads to a rotation of the pseudo spin of $-2\theta_{\mathbf{q}}$. (b) Relation between the STM tip position (M point) and the pseudospin rotation in intervalley backscattering by a H atom. The figure is adapted from Ref. [31].

their unusual $1/r^2$ decay for intravalley scattering ($\Delta\mathbf{K} = 0$ and $\xi = \xi'$) [14, 18, 19]. For intervalley scattering ($\Delta\mathbf{K} \neq 0$ and $\xi' = -\xi = -1$), there exist sub-wavelength anisotropic oscillations that are independent of the energy. If they exist on both sublattices (Figure 5a, b), the electron density on sublattice B has an additional phase shift $-2\theta_{\mathbf{r}}$, which is nothing but the pseudospin rotation associated with intervalley backscattering since $-2\theta_{\mathbf{r}} = -2\theta_{\mathbf{q}}$. Thus, the H adatom on sublattice A maps the phase singularity of the pseudospin at the Dirac cone apex into real space, and it acts as a 4π vortex for the charge density on sublattice B, as discussed above in the context of Figure 4a, b. The strength N of the dislocation is then given by the vortex charge, that is, the circulation of the gradient phase of the $\Delta\mathbf{K}$-wavevector oscillations around the adatom:

$$2\pi N = \oint_C \mathbf{dr}\cdot\nabla_{\mathbf{r}}(\Delta\mathbf{K}\cdot\mathbf{r} - 2\xi\theta_{\mathbf{r}}) = -2\oint_C \mathbf{dr}\cdot\nabla_{\mathbf{r}}(\xi\theta_{\mathbf{r}}) = 4\pi. \tag{5}$$

This explains the $N = 2$ wavefronts emerging from the H adatom in Figure 5b and shows explicitly that they reveal the pseudospin winding and so the Berry phase. This double dislocation splits into two single dislocations in the experiments (Figure 3d). This particular feature is recovered when taking into account the contributions of the two sublattices in the STM signal, as shown in Figure 5c.

5. Conclusions

The Berry phase π is a topological property that characterises a phase singularity of the wave-function pseudospin at the diabolic degeneracy point. So far experimental measurements in graphene relied on magnetic cyclotron orbits enclosing this phase singularity in momentum space. We have demonstrated instead that one can materialize the phase singularity directly in real space with an atomic scatterer. The scatterer acts as a vortex for the pseudospin of the scattering waves and is the source of wavefront dislocations in the LDOS. The dislocation strength then relates to the circulation of the wave-function pseudospin around the scatterer and so to the Berry phase around the phase singularity.

Phase singularities were known to be the source of wavefront dislocations, regardless of the wave equations. Wavefront dislocations are then ubiquitous from the physics of tides and sound

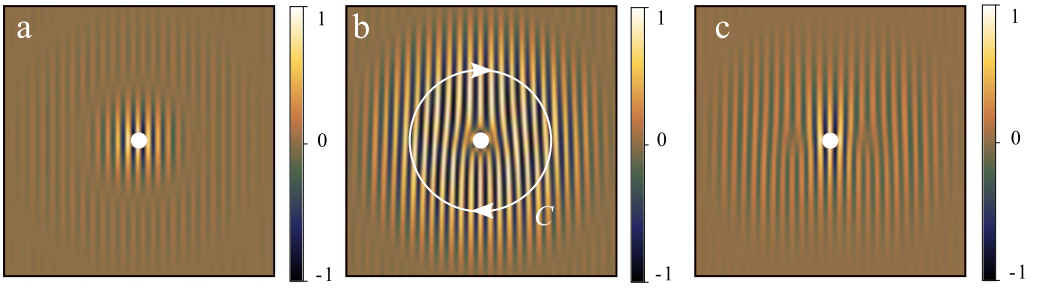

Figure 5. (a) Charge density modulation induced by intervalley scattering on sublattice A. (b) Charge density modulation induced by intervalley scattering on sublattice B. (c) Total charge density modulation induced by intervalley scattering and resulting from the two sublattice contributions. The modulations have been normalized to 1. The images are 10 nm × 10 nm and the signal is integrated from 0 eV to $V_b = 0.4$ eV. The white disk depicts the H adatom. The figure is adapted from Ref. [31].

to electromagnetism, singular optics, and quantum mechanics in connection to the Aharonov–Bohm wave function [32–38]. As in graphene, the phase singularities of electron wave-functions in solids are generally associated with the spectral degeneracy points of nodal band structures. Phase singularities are then at the heart of electronic properties of semimetals and topological insulators and superconductors. We then expect that topological defects in the wavefronts of LDOS fluctuations may also occur ubiquitously in such materials. This expectation is also supported by recent predictions and observations in other semimetallic and insulating systems, where wavefront dislocations also appear as evidence of the band-structure topology [39–42]. Thus, topological defects in the wavefronts of the LDOS around point scatterers appear as a promising alternative approach to identify topological materials in the experiments.

Acknowledgements

The authors thank P. Mallet, J.-Y. Veuillen and J. M. Gómez Rodriguez for experimental support. HG-H and IB were supported by AEI and FEDER under project MAT2016-80907-P (AEI/FEDER, UE), by the Fundación Ramón Areces, and by the Comunidad de Madrid NMAT2D-CM program under grant S2018/NMT-4511. MIK acknowledges a support of NWO via Spinoza Prize. CD acknowledges the support of Idex Bordeaux (Maesim Risky project 2019 of the LAPHIA Programme).

References

[1] Y. Aharonov, D. Bohm, "Significance of electromagnetic potentials in the quantum theory", *Phys. Rev.* **115** (1959), no. 3, p. 485-491.
[2] M. V. Berry, "Quantal phase factors accompanying adiabatic changes", *Proc. R. Soc. Lond. A* **392** (1984), no. 1802, p. 45-57.
[3] M. Berry, "Geometric phase memories", *Nat. Phys.* **6** (2010), no. 3, p. 148-150.
[4] F. Ghahari, D. Walkup, C. Gutiérrez, J. F. Rodriguez-Nieva, Y. Zhao, J. Wyrick, F. D. Natterer *et al.*, "An on/off Berry phase switch in circular graphene resonators", *Science* **356** (2017), no. 6340, p. 845-849.
[5] K. S. Novoselov, A. K. Geim, S. V. Morozov, D. Jiang, M. I. Katsnelson *et al.*, "Two-dimensional gas of massless dirac fermions in graphene", *Nature* **438** (2005), p. 197-200.
[6] Y. Zhang, Y.-W. Tan, H. L. Stormer, P. Kim, "Experimental observation of the quantum hall effect and Berry's phase in graphene", *Nature* **438** (2005), p. 201-204.
[7] M. F. Crommie, C. P. Lutz, D. M. Eigler, "Imaging standing waves in a two-dimensional electron gas", *Nature* **363** (1993), p. 524-527.

[8] P. T. Sprunger, L. Petersen, E. W. Plummer, E. Lægsgaard, F. Besenbacher, "Giant friedel oscillations on the beryllium (0001) surface", *Science* **275** (1997), no. 5307, p. 1764-1767.
[9] L. Petersen, P. T. Sprunger, P. Hofmann, E. Lægsgaard, B. G. Briner, M. Doering, H.-P. Rust *et al.*, "Direct imaging of the two-dimensional fermi contour: Fourier-transform STM", *Phys. Rev. B* **57** (1998), p. R6858-R6861.
[10] L. Petersen, B. Schaefer, E. Lægsgaard, I. Stensgaard, F. Besenbacher, "Imaging the surface fermi contour on cu (110) with scanning tunneling microscopy", *Surf. Sci.* **457** (2000), no. 3, p. 319-325.
[11] J. Friedel, "XIV. The distribution of electrons around impurities in monovalent metals", *Philos. Mag.* **43** (1952), no. 337, p. 153-189.
[12] N. Avraham, J. Reiner, A. Kumar-Nayak, N. Morali, R. Batabyal *et al.*, "Quasiparticle interference studies of quantum materials", *Adv. Mater.* **30** (2018), no. 41, article no. 1707628.
[13] G. M. Rutter, J. N. Crain, N. P. Guisinger, T. Li, P. N. First, J. a. Stroscio, "Scattering and interference in epitaxial graphene", *Science* **317** (2007), no. 5835, p. 219-222.
[14] I. Brihuega, P. Mallet, C. Bena, S. Bose, C. Michaelis, L. Vitali *et al.*, "Quasiparticle chirality in epitaxial graphene probed at the nanometer scale", *Phys. Rev. Lett.* **101** (2008), article no. 206802.
[15] P. Mallet, I. Brihuega, S. Bose, M. M. Ugeda, J. M. Gómez-Rodríguez, K. Kern, J. Y. Veuillen, "Role of pseudospin in quasiparticle interferences in epitaxial graphene probed by high-resolution scanning tunneling microscopy", *Phys. Rev. B* **86** (2012), article no. 045444.
[16] T. Ando, T. Nakanishi, "Impurity scattering in carbon nanotubes—absence of back scattering—", *J. Phys. Soc. Japan* **67** (1998), no. 5, p. 1704-1713.
[17] M. I. Katsnelson, K. S. Novoselov, A. K. Geim, "Chiral tunnelling and the Klein paradox in graphene", *Nat. Phys.* **2** (2006), p. 620-625.
[18] V. V. Cheianov, V. I. Fal'ko, "Friedel oscillations, impurity scattering, and temperature dependence of resistivity in graphene", *Phys. Rev. Lett.* **97** (2006), no. 22, article no. 226801.
[19] C. Dutreix, M. I. Katsnelson, "Friedel oscillations at the surfaces of rhombohedral *n*-layer graphene", *Phys. Rev. B* **93** (2016), no. 3, article no. 035413.
[20] J. N. Fuchs, F. Piéchon, M. O. Goerbig, G. Montambaux, "Topological Berry phase and semiclassical quantization of cyclotron orbits for two dimensional electrons in coupled band models", *Eur. Phys. J. B* **77** (2010), p. 351-362.
[21] J. R. Hahn, H. Kang, "Vacancy and interstitial defects at graphite surfaces: Scanning tunneling microscopic study of the structure, electronic property, and yield for ion-induced defect creation", *Phys. Rev. B* **60** (1999), p. 6007-6017.
[22] A. Hashimoto, K. Suenaga, A. Gloter, U. Koki, S. Iijima, "Direct evidence for atomic defects in graphene layers", *Nature* **430** (2004), p. 870-873.
[23] J.-H. Chen, W. G. Cullen, C. Jang, M. S. Fuhrer, E. D. Williams, "Defect scattering in graphene", *Phys. Rev. Lett.* **102** (2009), article no. 236805.
[24] F. Schedin, A. K. Geim, S. V. Morozov, E. W. Hill, P. Blake *et al.*, "Detection of individual gas molecules adsorbed on graphene", *Nat. Mater.* **6** (2007), no. 9, p. 652-655.
[25] T. O. Wehling, K. S. Novoselov, S. V. Morozov, E. E. Vdovin, M. I. Katsnelson *et al.*, "Molecular doping of graphene", *Nano Lett.* **8** (2008), no. 1, p. 173-177.
[26] D. C. Elias *et al.*, "Control of graphene's properties by reversible hydrogenation: evidence for graphane", *Science* **323** (2009), no. 5914, p. 610-613.
[27] R. R. Nair *et al.*, "Fluorographene: a two-dimensional counterpart of teflon", *Small* **6** (2010), no. 24, p. 2877-2884.
[28] O. V. Yazyev, L. Helm, "Defect-induced magnetism in graphene", *Phys. Rev. B* **75** (2007), article no. 125408.
[29] D. W. Boukhvalov, M. I. Katsnelson, A. I. Lichtenstein, "Hydrogen on graphene: Electronic structure, total energy, structural distortions and magnetism from first-principles calculations", *Phys. Rev. B* **77** (2008), article no. 035427.
[30] H. González-Herrero, J. M. Gómez-Rodríguez, P. Mallet, M. Moaied, J. J. Palacios *et al.*, "Atomic-scale control of graphene magnetism by using hydrogen atoms", *Science* **352** (2016), no. 6284, p. 437-441.
[31] C. Dutreix, H. Gonzàlez-Herrero, I. Brihuega, M. I. Katsnelson, C. Chapelier, V. T. Renard, "Measuring the Berry phase of graphene from wavefront dislocations in friedel oscillations", *Nature* **574** (2019), p. 219-222.
[32] J. F. Nye, M. V. Berry, "Dislocations in wave trains", *Proc. R. Soc. Lond. A* **336** (1974), no. 1605, p. 165-190.
[33] M. V. Berry, R. G. Chambers, M. D. Large, C. Upstill, J. C. Walmsley, "Wavefront dislocations in the Aharonov–Bohm effect and its water wave analogue", *Eur. J. Phys.* **1** (1980), no. 3, p. 154-162.
[34] M. V. Berry, "Making waves in physics", *Nature* **403** (2000), p. 21-21.
[35] M. R. Dennis, K. O'Holleran, M. J. Padgett, "Chapter 5 Singular optics: Optical vortices and polarization singularities", in *Progress in Optics*, vol. 53, Elsevier, Amsterdam, 2009, p. 293-363.
[36] J. Leach, M. R. Dennis, J. Courtial, M. J. Padgett, "Laser beams: Knotted threads of darkness", *Nature* **432** (2004), no. 7014, p. 165-165.
[37] M. Rafayelyan, E. Brasselet, "Bragg–Berry mirrors: reflective broadband q-plates", *Opt. Lett.* **41** (2016), no. 17, p. 3972-3975.

[38] M. V. Berry, "Gauge-invariant Aharonov–Bohm streamlines", *J. Phys. A: Math. Theoret.* **50** (2017), no. 43, article no. 43LT01.
[39] V. T. Phong, E. J. Mele, "Obstruction and interference in low energy models for twisted bilayer graphene", *Phys. Rev. Lett.* **125** (2020), article no. 176404.
[40] Y. Zhang, Y. Su, L. He, "Local Berry phase signatures of bilayer graphene in intervalley quantum interference", *Phys. Rev. Lett.* **125** (2020), no. 11, article no. 116804.
[41] C. Dutreix, P. Delplace, "Geometrical phase shift in friedel oscillations", *Phys. Rev. B* **96** (2017), no. 19, article no. 195207.
[42] C. Dutreix, M. Bellec, P. Delplace, F. Mortessagne, "Wavefront dislocations reveal the topology of quasi-1D photonic insulators", *Nat. Commun.* **12** (2021), article no. 3571.